

PAPER • OPEN ACCESS

Microstructure and strength of weldment in Pt20Rh alloys dispersion-strengthened by ZrO₂ particles

To cite this article: Faping Hu *et al* 2019 *IOP Conf. Ser.: Mater. Sci. Eng.* **580** 012035

View the [article online](#) for updates and enhancements.

You may also like

- [Effect of Catalyst and Catalyst Layer Composition on Catalyst Support Durability](#)
Siddharth Komini Babu, Rangachary Mukundan, Chunmei Wang et al.
- [Conductive polycrystalline diamond probes for local anodic oxidation lithography](#)
A J Ulrich and A D Radadia
- [Influence of the preparation conditions on the morphology and photocatalytic performance Pt-modified hexaniobate composites](#)
Barbara N Nunes, Antonio Otavio T Patrocínio and Detlef W Bahnemann

ECS
The
Electrochemical
Society
Advancing solid state &
electrochemical science & technology

DISCOVER
how sustainability
intersects with
electrochemistry & solid
state science research

Microstructure and strength of weldment in Pt20Rh alloys dispersion-strengthened by ZrO₂ particles

Faping Hu¹, Ziyang Wang¹, Tianbo Yu², Zonglun Yang³, Guobing Wei¹, Xuan Luo¹, Niels Hansen^{1,4}, Xiaoxu Huang^{1,2}, Weidong Xie^{1*}

¹ International Joint Laboratory for Light Alloys (MOE), College of Materials Science and Engineering, Chongqing University, Chongqing 400044, China;

² Department of Mechanical Engineering, Technical University of Denmark, DK-2800 Kgs. Lyngby, Denmark

³ Chongqing Polycomp International Corporation, Chongqing 400044, China

⁴ Technical University of Denmark, Risø Campus, DK-4000 Roskilde, Denmark

E-mail: wdxie@cqu.edu.cn

Abstract. A series of Pt20Rh alloys dispersion-strengthened by different volume fractions of ZrO₂ particles have been prepared by internal oxidation of Pt20Rh powder followed by consolidation and hot forging. The alloys were cold rolled to sheets, followed by annealing. The effects of welding on the microstructure and mechanical properties were also investigated. The microstructure of the rolled sheets showed a lamellar structure and the yield stress was significantly increased with increasing volume fraction of dispersion particles. After welding, the yield stress at room temperature was almost unchanged, although a small decrease was observed at 1000 °C. However, the work hardening capacity and ultimate tensile stress were significantly reduced in the welded sample due to grain coarsening and to increased pore density in the fusion zone.

1. Introduction

Platinum is characterized by a high melting point combined with excellent chemical inertia [1-3]. These properties are particularly useful in the glass industry where platinum is the main metal for manufacturing bushing, i.e. a platinum container used in the manufacture of continuous glass fibers. The bushing is exposed to an aggressive service environment (high temperature range from 1100 °C to 1400 °C, alternating loads with a stress between 1 MPa to 40 MPa, contact with molten glass and air, etc.) for typically more than one year [3-5]. However, pure platinum is relatively soft at room temperature, and even softer after high temperature exposure due to grain growth.

An innovative preparation route that combines powder metallurgy and internal oxidation has been proven to be very effective for strengthening of platinum-based alloys [4, 6], in which the alloys are produced by consolidation of milled powder that has been internally oxidized. To widen the industrial application of the material its weldability is important. For example, in the fiber glass industry, the bushing is a rectangular open topped box having a base with typically 1000 – 4000 precisely shaped orifices with bore diameters from 1.1 mm up to 2.5 mm and lengths 2.25 times their bore diameters [5]. To construct this bushing the base and the orifices are fabricated separately, followed by a manual welding during processing. As a result, the weldment will be composed of different zones with



different structure and mechanical properties. These zones can be characterized as: (i) the fusion zone (FZ); (ii) the heat affected zone (HAZ); and (iii) unaffected base metal (BM). In combination, the presence of these zones may weaken the material by reducing fracture toughness and high temperature strength.

In the present work dispersion-strengthened platinum alloys with various volume fractions of ZrO₂ have been produced by internal oxidation-powder metallurgy processes and arc welded to explore the effects of welding on the microstructure and strength properties.

2. Experimental procedures

Table 1 shows the nominal composition of investigated alloys. Sheets of Pt20Rh, 1 mm in thickness, containing different amounts of ZrO₂, were prepared by internal oxidation-powder metallurgy processes as described in a previous paper [6] and were welded along the transverse direction (TD). The welding parameters (manual arc welding with no filler metal) are given in table 2.

Table 1. Composition of the investigated alloys (in weight %).

Alloys	Zr	Y	Others	Rh	Pt
A	–	0.015	≤0.01	20	Bal.
B	0.05	0.015	≤0.01	20	Bal.
C	0.10	0.015	≤0.01	20	Bal.
D	0.30	0.015	≤0.01	20	Bal.

Table 2. Welding parameters.

Weld parameters	
Argon flow	3-4 L/min
Current	30-50 A
Weld speed	12-17 cm/min

The weldments and their unwelded BM were machined into dog-bone shape tensile samples (gauge section of 20 mm, 10 mm and 1 mm in length, width and thickness, respectively) taken along the rolling direction. Tensile tests were conducted at an initial strain rate of $8.3 \cdot 10^{-3} \text{ s}^{-1}$ at RT and of $8.3 \cdot 10^{-5} \text{ s}^{-1}$ at 1000 °C. The samples were cut so that about 3 mm of weld line was located in the mid-gauge position of the tensile specimen for each weldment.

To characterize the microstructure of the samples, scanning electron microscopy (FEI Nova 400 FEG, and Zeiss Supra 35 equipped with electron backscatter diffraction detector) and transmission electron microscopy (JEOL JEM-2100) were carried out. The samples for SEM observations were prepared by mechanical grinding and polishing. The sizes and area of the pores were measured by the Image-Pro Plus6 (IPP) software. Mechanical grinding and ion thinning were used in the preparation of TEM samples. For simplicity, the alloys are referred to hereafter as A (0 wt%Zr), B (0.05 wt%Zr), C (0.1 wt%Zr) and D (0.3 wt%Zr).

3. Results

3.1 Mechanical properties

All weldments fractured at the welding line, both during tensile testing at room temperature and at 1000 °C. Figure 1 shows the engineering stress-engineering strain curves at room temperature, which indicates that the yield stress (0.2% proof, $\sigma_{0.2}$) and the ultimate tensile stress (UTS) of the BM are

significantly increased with increasing ZrO₂ content, accompanied by a slight decrease in total elongation. After welding, the initial part of the tensile curve of each weldment was basically the same as its BM, but failure occurred at a much lower strain in the weldment than in the BM. As a result, the $\sigma_{0.2}$ yield stress of each weldment is almost the same as its BM, but the total elongation and UTS of each weldment are clearly reduced compared with the BM, although the elongation of weldment is still acceptable. The measured values of $\sigma_{0.2}$, UTS and total elongation of the investigated samples are shown in table 3.

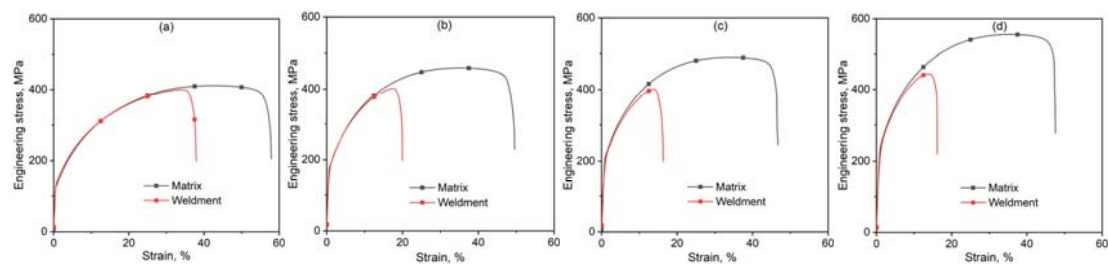


Figure 1. Stress-strain curves of samples A (a), B (b), C (c) and D (d) and their welded counterparts at room temperature.

Figure 2 shows the engineering stress-strain curves at 1000°C, indicating that the strength and elongation of both weldments and their BMs are significantly decreased, compared to their room-temperature counterparts. After welding, the elongation to failure for the weldments is dramatically reduced compared to the corresponding BM, ranging from 7% to 2% with increasing ZrO₂ particle concentration. Furthermore, the $\sigma_{0.2}$ of the BM and of the weldments are significantly raised with increasing ZrO₂ content, and the $\sigma_{0.2}$ of each weldment is close to that of its BM although a slight decrease was observed in samples C and D, which are similar with room-temperature tensile results.

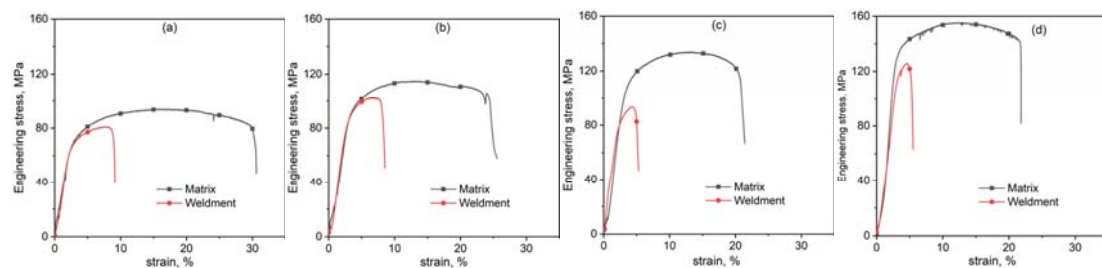


Figure 2. Engineering stress-strain curves of samples A (a), B (b), C (c) and D (d) and their weldments during tensile testing at 1000 °C.

Table 3. Tensile properties (BM/weldment) of the investigated samples at RT and at 1000 °C.

Alloy	$\sigma_{0.2}$, MPa		UTS, MPa		Total elongation, %	
	RT	1000 ° C	RT	1000 ° C	RT	1000 ° C
A	143/146	67/66	411/400	91/81	57/37	28/7
B	200/196	89/87	459/402	114/102	49/19	22/6
C	228/218	99/82	491/401	137/94	46/15	17/3
D	256/236	124/113	555/445	152/124	46/15	18/2

3.2 Microstructure

ZrO₂-strengthened Pt20Rh alloys possess an excellent thermal stability and basically no recrystallization occurs after annealing at 1150 °C for 30 min, as shown in figure 3a, where the morphology of the BM was characterized by high angle boundaries (HABs) approximately parallel to TD and low angle boundaries (LABs) distributed between the HABs, indicating a recovered, lamellar structure. After welding, two new zones were developed, namely the HAZ and FZ, as shown in figures 3b and 3c. The grains in the HAZ are fully recrystallized with a slightly elongated shape along TD, while the grains in FZ are as-cast dendrites. Furthermore, a large number of LABs are observed in both the HAZ and FZ, but their distribution is non-uniform.

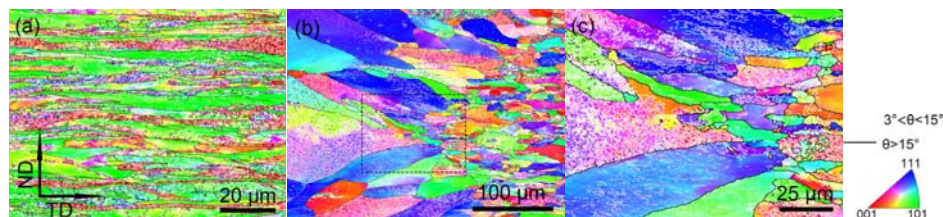


Figure 3. EBSD inverse pole figure (IPF) with respect to the RD of sample C: (a) the BM; (b) the transition region between HAZ (right) and FZ (left); (c) magnified area of the rectangle marked by dotted lines in (b). Black lines and white lines indicate HABs and LABs, respectively.

Due to the powder metallurgy process, the formation of pores within the alloys seems inevitable. Figure 4 shows the morphology of the pores in the BM (a, c and e) and FZ (b, d and f) of the investigated alloys, and figure 5 shows distributions of pore diameters. The pores are approximately spherical and basically uniformly distributed. The porosity in the BM (FZ) for samples A, C and D are 0.18% (0.41%), 0.26% (0.54%), and 0.68% (1.29%), respectively. It is obvious that both the porosity and the pore size increase with increasing ZrO₂ particle content in the BM regions. After welding, the porosity in the FZ was approximately doubled for each sample. The frequency of smaller pores (0 - 0.2 μm) significantly decreased while that of larger pores (>0.2 μm) increased.

Figure 6 shows the representative particle morphology in samples A (a) and C (b) in the FZ. Spherical particles were found in these two alloys and no obvious aggregation was detected. In our recent studies, the particles in sample A have been identified as yttria, while the particles in the other alloys (samples B, C and D) were identified as ZrO₂ with either a monoclinic structure or a tetragonal structure.

4. Discussion

Based on the results of the tensile tests, the Pt20Rh strengthened by various ZrO₂ particle concentrations basically maintained their yield stress after fusion welding both at room temperature and at 1000 °C, while the work hardening capability was dramatically decreased, especially at 1000 °C. The microstructural analysis showed that three aspects may be responsible for these phenomena.

The BM regions of the investigated alloys have a recovered structure with lamellar HABs that are divided by LABs. During arc welding, the metal in the FZ underwent a melting process followed by solidification and developed into a cast structure characterized by coarse grains that weaken the alloy according to Hall-Petch relationship [7]. However, based on EBSD results, there are also numerous LABs formed within the resolidified grains, which may be ascribed to the high welding temperature [8] and good electrical conductivity and therefore rapid solidification. These LABs can impede dislocation movement and strengthen the alloys [9]. It should be noted that the distribution of LABs is non-uniform and some coarse grains containing a few LABs are weaker. These weaker grains may lead to premature fracture during deformation and cause failure of the whole sample.

Pores within a metal are usually detrimental to its strength and ductility because they reduce the stressed area and cause stress concentration, both of which effects are enhanced with increasing pore

size and porosity. Furthermore, pore shape also affects the mechanical properties of a metal with usually a smaller dihedral angle resulting in easier cracking, due to increased stress concentration. Fortunately, the pores in the investigated alloys are relatively fine, spherical and homogeneously distributed, though they are increased in number and enlarged with increasing particle content or after welding. Thus, at the initial stage of deformation, these fine pores can act as obstacles for dislocations motion. With increasing deformation, however, the pores may gradually become crack sources due to stress concentrations caused by accumulative dislocations around the pores.

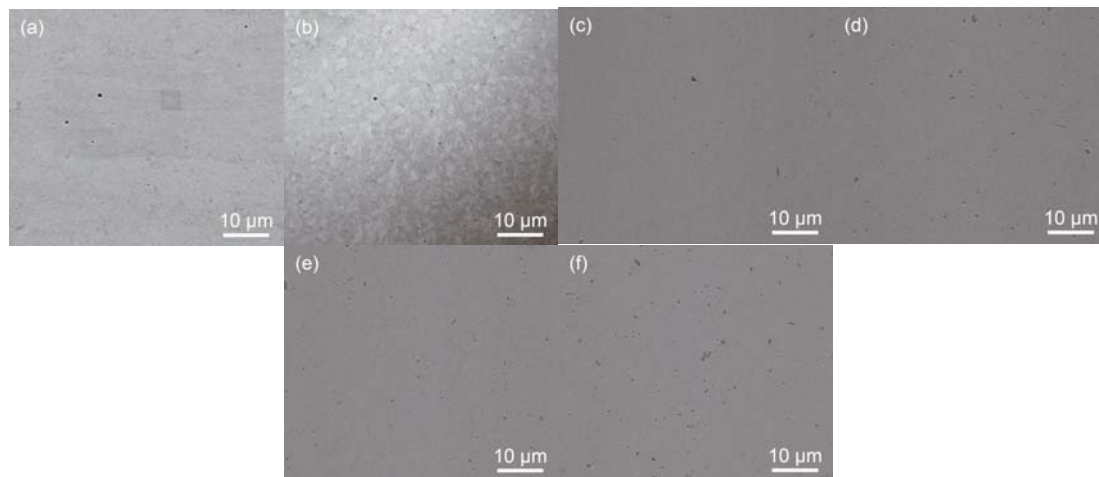


Figure 4. SEM images showing the microstructure in the HAZ and FZ of sample A (a, b), sample C (c, d) and sample D (e, f).

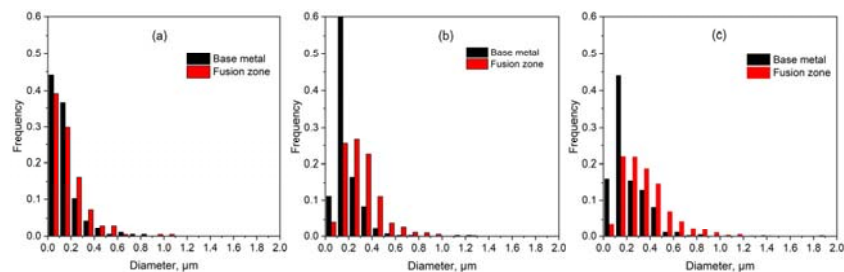


Figure 5. Pore size distributions in the BM and FZ of samples A (a), C (c) and D (c).

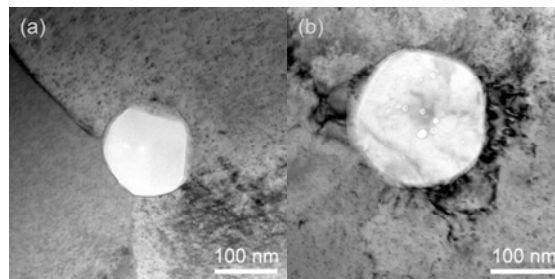


Figure 6. TEM bright field images showing particles in sample A (a) and C (b).

Impenetrable particles in a metal can effectively strengthen the metal both at room temperature and at high temperature by hindering dislocation motion. To pass through the particles, a dislocation must

bow out between the particles, therefore increasing the yield stress of the metal, which is well described by the Orowan equation, where the increment of yield stress is positively correlated to the particle spacing [10]. Thus, as shown in figures 1 and 2, the yield stress of the investigated alloys was significantly increased with increasing impenetrable ZrO₂ particle concentration. After welding, the particles basically maintained their spherical shape and no obvious segregation was detected. This may be an important reason to explain why the yield stress of the alloys is basically unchanged after welding.

5. Conclusions

Pt20Rh alloys strengthened by ZrO₂ particles with various volume fractions have been prepared and welded. The effects of welding on microstructure and tensile properties at room temperature and at 1000 °C have been investigated. The conclusions are as follows.

1. The yield stress of Pt20Rh significantly increased with increasing ZrO₂ particle content. After welding, each weldment basically maintained its yield stress compared to the BM both at room temperature and at 1000 °C, while its work hardening capability was significantly decreased.
2. After welding, the initial recovered structure developed into an as-cast coarse grain structure in the FZ which was divided by non-uniform LABs caused by rapid cooling. Fine, spherical and homogeneously distributed pores were formed during the powder metallurgy process, whose area and size were increased with increasing particle content and after welding. Particles were observed to be spherical in the investigated alloys without obvious segregation.
3. LABs and uniformly distributed particles in the FZ should be responsible for the basically unchanged yield stress before and after welding, while the significant decline in total elongation and UTS may be the result of coarsened grains and increased pore density in the FZ.

Acknowledgements

Financial support from the Chongqing Science and Technology Bureau of China through Grant cstc2017zdcy-zdyfX0070 and cstc2018jszx-cydzX0138 as well as the European Research Council (ERC) under the European Union's Horizon 2020 research and innovation program through Grant agreement No 788567 is gratefully acknowledged.

Reference

- [1] Hu B X, Ning Y and Chen L 2012 *Platin. Met. Rev.* **56** 40.
- [2] Chen H, Xie W and Liu W T 2018 *Vacuum* **160** 445.
- [3] Selman G L, Day J G and Bourne A A 2018 *Platin. Met. Rev.* **18** 46.
- [4] Maruyama K, Yamasaki H and Hamada T 2009 *Sci. Eng. A* **510** 312.
- [5] Stokes J 1987 *Platin. Met. Rev.* **31** 54.
- [6] Dai Y, Ma Q and Liu W T 2018 *Mater. Sci. Tech.* **34** 654.
- [7] Hansen N 2013 *Scripta Mater.* **51** 801.
- [8] Okamoto H 2013 *J. Phase Equilib. Diff.* **34** 176.
- [9] Huang T, Shuai L and Wakeel A 2018 *Acta Mater.* **156** 369.
- [10] Hansen N 1997 *Acta Metal.* **25** 863.